BIOCHEMISTRY
including biophysical chemistry & molecular biology
Article

Biochemistry **2009,** *48,* 8817–8829 8817
DOI: 10.1021/bi900703v

The ALS-Associated Mutation G93A in Human Copper-Zinc Superoxide Dismutase Selectively Destabilizes the Remote Metal Binding Region[†]

Anna Katrine Museth,[‡] Ann-Christin Brorsson,[‡] Martin Lundqvist,[‡] Lena A. E. Tibell,*[,§] and Bengt-Harald Jonsson*[,‡]

[‡]*Division of Molecular Biotechnology, Department of Physics, Chemistry and Biology, Linköping University, SE-581 83 Linköping, Sweden, and* [§]*Department of Science and Technology, Linköping University, SE-601 74 Norrköping, Sweden*

Received April 24, 2009; Revised Manuscript Received August 2, 2009

ABSTRACT: More than 100 distinct mutations in the gene (SOD1) for human copper-zinc superoxide dismutase (CuZnSOD) have been associated with familial amyotrophic lateral sclerosis (fALS). Studies of these mutant proteins, which often have been performed under far from physiological conditions, have indicated effects on protein stabilities, catalytic activity, and metal binding affinities but with no common pattern. Also, with the knowledge that ALS is a late onset disease it is apparent that protein interactions which contribute to the disorder might, in the natural cellular milieu, depend on a delicate balance between intrinsic protein properties. In this study, we have used experimental conditions as near as possible to the in vivo conditions to reduce artifacts emanating from the experimental setup. Using $^{1}H-^{15}N$ HSQC NMR spectroscopy, we have analyzed hydrogen exchange at the amide groups of wild-type (wt) CuZnSOD and the fALS-associated G93A SOD variant in their fully metalated states. From analyses of the exchange pattern, we have characterized the local dynamics at 64% of all positions in detail in both the wt and G93A protein. The results show that the G93A mutation had no effect on the dynamics at a majority of the investigated positions. However, the mutation results in local destabilization at the site of the mutation and also in stabilization at a few positions that were apparently scattered over the entire protein surface. Most remarkably, the mutation selectively destabilized the remote metal binding region. The results indicate that the metal binding region may affect the intermolecular protein−protein interactions which cause formation of protein aggregates.

Like other common neurodegenerative diseases, e.g., Alzheimer's disease, Parkinson's disease, and Huntington's disease, amyotrophic lateral sclerosis (ALS)[1] is characterized by mid-to-late-life onset, selective neuronal death, and the formation of protein deposits in affected neuronal tissues (*1*). This progressive neurodegenerative disease results in a gradual degradation of motor neurons in the motor cortex, brain stem, and spinal cord (*2*). The general prognosis for ALS is a median age at onset of 46 years (range of 24−72 years) and a median duration of disease of 3.0 years (range of 0.3−20 years) (*3*).

Most cases of ALS are sporadic, i.e., occurring in individuals with no family history of ALS. However, a genetic link has been found in roughly 10% of all reported cases of the disease. Collectively, they are termed familial ALS (fALS). Of these cases, approximately one in five has been directly attributed to autosomal dominant mutations in the gene (SOD1) that encodes the intracellular copper-zinc superoxide dismutase (CuZnSOD) (*4*−*6*). More than 100 distinct SOD1 mutations (*7*) have been identified in fALS patients. Most of the individual ALS-linked mutations in CuZnSOD result in substitution of one amino acid; however, there are also a smaller group of mutations resulting in amino acid deletions and truncations. An intriguing aspect is that mutations are found throughout the gene and have been identified at more than one-third of the 153 amino acid residues of the wild-type (wt) CuZnSOD protein, yet in most instances, these mutations do not significantly lower the SOD activity of the resulting enzyme (*8*).

At present, the mechanism or mechanisms whereby mutations in the gene encoding CuZnSOD cause the disease are unknown. However, a major insight into the role of CuZnSOD in fALS was gained when Gurney et al. (*9*) found that transgenic mice expressing the fALS mutant G93A CuZnSOD developed progressive motor neuron disease despite having high levels of SOD activity. In addition, transgenic mice with no endogenous CuZnSOD were found not to develop motor neuron disease, suggesting that SOD-associated fALS is not associated with a change in SOD activity but rather is caused by a toxic gain of function induced by the ALS mutant CuZnSOD protein (*10*). Several models for how the neurodegenerating toxicity in ALS arises include binding of mutant SOD to heat shock proteins (*11*) with the subsequent prevention of their antiapoptotic function (*12*) and formation of toxic SOD aggregates (*13*−*16*). Transgenic mice expressing human G93A CuZnSOD have shown progressive aggregation of the G93A CuZnSOD and ubiquitin in the perikarya of spinal cord motor neurons and fragmentation of the neural golgi apparatus (*17*, *18*). The aggregation hypothesis maintains that mutant CuZnSOD proteins are, or become, misfolded and consequently aggregate into increasingly high-molecular weight species that ultimately lead to the death of motor neurons. It has been argued that structural destabilization,

[†]This study was supported by a grant (621-2006-4253) from the Swedish Research Council to B.-H.J.

*To whom correspondence should be addressed. L.A.E.T.: phone, +4611363376; fax, +4611363270; e-mail, lena.tibell@liu.se. B.-H.J.: phone, +4613288935; fax, +4613282399; e-mail, nalle@ifm.liu.se.

[1]Abbreviations: ALS, amyotrophic lateral sclerosis; CuZnSOD, human copper-zinc superoxide dismutase; SOD1, gene for human copper-zinc superoxide dismutase; G93A, replacement of glycine with alanine in position 93 in CuZnSOD.

Published on Web 08/05/2009

metal depletion, reduction of disulfide bonds, and/or a change in the dynamic properties of CuZnSOD mutants may play a role in the pathology of CuZnSOD-related ALS (*13*, *19*−*25*).

The human CuZnSOD is a homodimeric protein with a subunit molecular mass of a 32 kDa containing one copper and one zinc ion per subunit. The copper ion in the enzyme mediates the disproportionation of superoxide anion to hydrogen peroxide and dioxygen ($2O_2^- + 2H^+ \rightarrow O_2 + H_2O_2$) in a reduction−oxidation cycle between Cu(I) and Cu(II) (*26*). CuZnSOD is an abundant protein (1−2% of the total protein content in the cell) and participates in the primary defense against superoxide anion radicals (a byproduct of aerobic metabolism) (*27*). The tertiary structure of CuZnSOD is a Greek key β-barrel with one intramolecular disulfide bridge in each subunit (*28*, *29*). Both these properties contribute to the high stability of the protein, which is highly resistant to thermal denaturation, detergent denaturation, and proteolysis (*30*).

Expression of recombinant human CuZnSOD (in *Escherichia coli*) was first reported in 1985 (*31*), and recombinant expression in *E. coli* in yeast (*32*) and baculovirus systems (*33*) has also been described. However, these production systems have resulted in a low level of metallization which has been a serious problem for the production of active ALS-associated CuZnSOD variants. Earlier studies of the most prominent CuZnSOD fALS mutants have therefore often been hampered by low metal content. However, the discovery or the network of copper-trafficking genes required for the incorporation of copper into proteins in vivo (*34*, *35*) led us to the development of a system for coexpression of CuZnSOD and the copper chaperone from yeast (yCCS). This system overproduces SOD variants with practically full Cu^{2+} content, which is a prerequisite condition for this study (*36*).

Biophysical studies of different ALS-associated variants of CuZnSOD have been performed under many different conditions, and these studies show that the SOD variants are diverse in characteristics such as melting temperature, Cu and Zn binding affinity, and net charge. Therefore, it has been suggested that SOD variants are likely to aggregate for different reasons or for distinct combinations of reasons (*37*−*40*). Thus, structural changes associated with the different mutations can be small and delicate and may escape detection in the structure determination by X-ray crystallography, and the dynamical effects at longer time scales might also escape detection upon analysis of magnetization relaxation properties by nuclear magnetic resonance spectroscopy (*41*). Furthermore, earlier biophysical studies of the ALS-associated CuZnSOD variants have in most cases been performed using pseudo-wild-type protein or ALS-associated CuZnSOD variants with additional point mutations, and the environmental conditions have often been far from physiologically relevant.

In this study, we aim to gain an understanding of the intrinsic dynamical and structural differences between the wt of CuZnSOD and the ALS-associated variant G93A. Since it seems apparent that the reasons for aggregation may depend on a delicate balance between intrinsic dynamical, structural, and chemicophysical properties and environmental factors, we use wt CuZnSOD, with no alterations in any position, and the ALS-associated variant G93A which is altered at position 93 only in our study. We also attempt to find conditions that are as close as possible to the natural physiological conditions in the cell, but still allowing measurements by high-resolution two-dimensional (2D) NMR methods. Hydrogen−deuterium (H−D) exchange experiments with these proteins were performed at pH 7, and they were monitored by $^1H-^{15}N$ HSQC consecutive NMR measurements.

MATERIALS AND METHODS

Expression and Purification of ^{15}N Human Intracellular CuZnSOD and ^{15}N Mutant G93A. For this purpose, the pSOD1 plasmid with an additional insert of the gene encoding the yeast copper charperone γCCS (*36*) was used and introduced into *E. coli* strain BL21/DE3. The use of this construct results in full incorporation in SOD (*36*). The G93A mutation was constructed previously by Lindberg et al. (*25*).

The cells were grown at room temperature to an OD_{600} of 0.5−0.6 in minimal medium [Na_2HPO_4 (6 g/L), KH_2PO_4 (3 g/L), NaCl (0.5 g/L), 40% (w/v) glucose (10 mL/L), $FeSO_4$ (0.01 mM), K_2SO_4 (0.28 mM), $CaCl_2$ (0.5 μM), $MgCl_2$ (1 mM), micrometer-utrients excl. $CoCl_2$ (1 mL/L), vitamin mixture (1 μg/L), and $^{15}NH_4Cl$ (0.5 g/L)] containing 100 mg/L ampicillin. At the time of induction, 0.5 mM IPTG and $CuSO_4$ and $ZnSO_4$ were added to final concentrations of 0.1 and 1 mM, respectively. Two hours before cells were harvested, additional $CuSO_4$ was added to a final concentration of 1 mM to ensure full and correct incorporation of the copper metal. The cells were harvested at 4 °C by centrifugation (3600 rpm), resuspended in 20 mM potassium phosphate buffer (pH 7.0) containing DNase and RNase, and lysed by ultrasonication (Misonix). After centrifugation (14900*g* for 45 min), ammonium sulfate (390 g/L supernatant) was added to the supernatant and stirred on ice for ~2 h before further centrifugation (14900*g* for 45 min). The supernatant was applied on a 50 mL Phenyl Sepharose 6 FF column (Amersham Biocensors) equilibrated with 2 M $(NH_4)_2SO_4$, 150 mM NaCl, and 50 mM KP_i (pH 7.0). The protein solution was washed with 150 mL before being eluted with 150 mM NaCl and 50 mM KP_i (pH 7.0) (from 0 to 100% in 300 mL). The protein eluted at ~60%. The purified protein fractions were dialyzed and concentrated. Samples for H−D exchange experiments were further lyophilized.

NMR Instrumentation and H−D Exchange. To assess H−D exchange, $^1H-^{15}N$ HSQC spectra were recorded consecutively over 4.5 days using a Varian Oxford AS600 NMR instrument. The spectra were collected at 600 MHz and 298 K; 2048 (^1H) × 256 (^{15}N) data points were acquired with spectral windows of 8000 Hz (^1H) and 2000 Hz (^{15}N) for each spectrum, corresponding to an acquisition time of 50 min.

Sample Preparation for H−D Exchange. The lyophilized protein, sodium isoascorbate, and a D_2O buffer (99% D_2O) containing 0.02 M potassium phosphate and 0.07 M K_2SO_4 (pH 7.0) were placed overnight in a glovebox with a nitrogen atmosphere to produce an anaerobic environment. The following day, the lyophilized protein sample was dissolved in 625 μL of the D_2O buffer, of which 600 μL was transferred to the NMR tube and maintained at 25 °C. To reduce the Cu(II) ions to Cu(I), sodium isoascorbate was dissolved in D_2O buffer to a concentration 100 times greater than that of the protein (dimer), and 25 μL was added to the NMR tube, resulting in a 4-fold excess of the isoascorbate over protein.

Data Evaluation. To process the data, NMRview 5.0 was used and the peaks were assigned on the basis of previous assignments done by Banci et al. (*42*). The exchange rates (k_{ex}) were determined by fitting the measured time-dependent cross-peak volume to single-exponential decays using Origin, and the corresponding ΔG values were calculated as described in the

Supporting Information. The highly recognized model for hydrogen−deuterium exchange of amide protons in aqueous solutions was formulated by Linderstrøm-Lang in the early 1950s (*43*). The model is based on the idea that amide protons (NH), if exposed to solvent water, constantly exchange with the protons in the surrounding water molecules. However, in native proteins, numerous amide protons are not directly exposed to solvent water since they either are located in the inside of the protein and therefore inaccessible to surface water or participate in a hydrogen bond and are thereby stabilized. A local opening or unfolding event, allowing the entrance of a water molecule, has to take place before H−D exchange can happen. Therefore, measurement of the H−D exchange rate can be used to characterize both local and global dynamics in proteins. A more detailed description of the theory and methodology can be found in the Supporting Information and in Bai et al. (*44*).

The consequences of EX1 and EX2 exchange mechanisms which are described in the Supporting Information are both indicated in the article by presenting k_{ex} (and $t_{1/2}$) which is the equal to the opening rate in the EX1 limit and ΔG, which is calculated assuming EX2 conditions. Since we have chosen to perform the experiments under near-physiological conditions at pH 7 only, it is not possible to distinguish between the two cases. A recent study by Jaswal and Miranker (*45*) indicates that for many proteins the exchange behavior at pH 7 is in a range between that of EX1 and EX2. Therefore, we have chosen to discuss both the half-life ($t_{1/2}$) and the ΔG values. One should note that the focus in the article is on a comparison between the wt SOD and the G93A variant. Since the comparison is made pairwise, residue by residue, all assumptions about the exchange mechanism cancel out.

RESULTS

Each of the two identical subunits in SOD contains 153 amino acids, of which six are proline. CuZnSOD is a relatively large protein to be assessed by 2D NMR, and therefore, signal overlaps were present. Despite the overlap of many of the NH signals in the 2D $^{15}N-^{1}H$ HSQC spectrum, it was possible to track the H−D exchange for 100 (65%) of the backbone NH signals as shown in Tables 1 and 2. The experiments were performed at pH 7.0 and 25 °C with an ionic strength near the physiological ionic strength to create conditions as close to in vivo conditions as possible. In the HD experiment, 2D $^{15}N-^{1}H$ HSQC spectra were recorded consecutively over a time period of 4.5 days. The processing time for each spectrum was set to 50 min. Thus, it was possible to determine the decay in signals for NH groups with half-lives between 25 min and 18 days corresponding to k_{obs} in the interval from 2.6×10^{-5} to 2.8×10^{-2} min^{-1}. Both wt SOD and the fALS SOD G93A mutant were investigated, and the results are described and compared in the following sections.

Exchange Patterns for wt CuZnSOD. All the results for wt CuZnSOD are listed in Table 1, and the exchange pattern is visualized in Figure 1. The structures and hydrogen bonding patterns which are indicated in the figures were taken from ref *46* [Protein Data Bank (PDB) entry 2C9V]. Thirty-three of the 100 investigated NH backbone signals exhibited a very rapid exchange with signals not detectable in the first spectrum ($t_{1/2}$ < 25 min). For 28 of the backbone NH signals, it was possible to determine the exchange rates. Rapid exchange (25 min < $t_{1/2}$ < 1 h) was observed for five of these, and nine residues exhibited intermediate exchange and were visible for approximately 1 day (1 h < $t_{1/2}$ < 24 h); the exchange rates for 14 residues were comparatively slow (24 h < $t_{1/2}$ < 18 days), leading to a signal remaining for more than 4.5 days. For 39 of the NH groups, primarily positioned in β-strands, no measurable reduction in signal intensity took place during the period of 4 days. From comparisons of exchange rates and the corresponding errors, it was found that the slowest exchange that could reliably be measured gave a $t_{1/2}$ of 18 days. Therefore, we have set the cutoff to 18 days ($t_{1/2}$ > 18 days).

β-Sheet Motif. The majority of the amide protons in the β-sheets exhibited slow exchange (blue and green in Figure 1). A greater part of these are involved in inter-β-strand hydrogen bonds according to the crystal structure (*46*) (PDB entry 2C9V). Earlier NMR studies have shown a high correlation in secondary structure between X-ray and NMR studies (*42*). The most stable parts of the β-structure were found between β-strand I and β-strand II, between β-strand II and β-strand III (except Val17, Ser34, and Lys36), between β-strand IV and β-strand VII, and finally between β-strand VII and β-strand VIII where no measurable H−D exchange took place ($t_{1/2}$ > 18 days). The structure between β-strand III and β-strand VI and between β-strand IV and β-strand V appeared to be slightly less stable where some of the protons exchange within the period from 24 h to 18 days. β-Strand I, β-strand VIII, and the C-terminal part are connected by a network of hydrogen bonds. This connection was reflected by the high stability found for Val5, Val7, and Gly150 ($t_{1/2}$ > 18 days) and also by the moderate stability found for Ala152 ($t_{1/2}$ = 1.7 days) and Cys146 ($t_{1/2}$ = 8.6 h). Notably, Val5 is stabilized by hydrogen binding to Gly150 positioned in β-strand VIII. Interestingly, Val7 was also very stable during the H−D experiment with no measurable exchange during the experimental time despite the indication from the crystal structure that Val7 forms a hydrogen bond to a network of surrounding water molecules only. This would indicate that the deep burial of the NH group of Val7 in the dimer interface is sufficient to protect it from rapid exchange. Alternatively, Val7 could form a hydrogen bond to Val148, since the "odd-numbered neighbors" Lys9 and Val5 are binding to Cys146 and Gly150. Regardless of the precise interaction, the result suggests that the interface area is rigid and stable.

The open end of the β-strand II−β-strand III hairpin that involves Val17, Ser34, and Lys36 exhibited a surprisingly high flexibility despite the presence of hydrogen bonds identified in the crystal structure. However, in the crystal structure, a significantly longer distance was found for the hydrogen bond between the NH and CO groups of Val17 and Ser34 than what is energetically favorable. Thus, it seems as if this part of the β-strand II−β-strand III hairpin exhibits local breathing dynamics.

Residues Asp83 and Leu84 are not directly involved in a normal β-sheet hydrogen bond network, but the slow exchange found for these amino acids can be explained by their hydrogen bonding to His80 and Gly82, respectively.

Asn86, Thr88, Glu100, and Arg143 which are positioned at the edge of their respective β-sheet motif exhibited fast exchange ($t_{1/2}$ for Asn86 of 46 min, and $t_{1/2}$ for Thr88, Glu100, and Arg143 of < 25 min). In line with these observations, no defined hydrogen bond partner for these residues has been found in the crystal structure. The edge residue Cys146 in β-strand VIII exhibited a surprisingly high stability ($t_{1/2}$ = 8.6 h) which can be explained by a hydrogen bond to the backbone carbonyl of Lys9 in β-strand I.

H−D Exchange for Residues in Loops and Coils. There was no common exchange pattern for residues in loops and coils.

Table 1: H−D Exchange Parameters for wt CuZnSOD[a]

	k_{ex} (min^{-1})	$t_{1/2}$ (min)	k_{ch} (min^{-1})	K_{op}	ΔG_{op} (kcal mol^{-1} L^{-1})		k_{ex} (min^{-1})	$t_{1/2}$ (min)	k_{ch} (min^{-1})	K_{op}	ΔG_{op} (kcal mol^{-1} L^{-1})
Ala1	−	−	1.9×10^3	−	−	Glu78	$> 2.8 \times 10^{-2}$	$< 2.5 \times 10$	7.9×10^3	$> 3.5 \times 10^{-6}$	< 7.4
Thr2	−	−	1.6×10^3	−	−	Arg79	3.8×10^{-3}	$1.8 \times 10^2 \pm 6 \times 10^0$	5.5×10^3	6.9×10^{-7}	8.4
Lys3	$> 2.8 \times 10^{-2}$	$< 2.5 \times 10$	2.7×10^3	$> 1.0 \times 10^{-5}$	< 6.8	His80	$< 2.6 \times 10^{-5}$	$> 2.7 \times 10^4$	2.5×10^3	$< 1.1 \times 10^{-8}$	> 10.9
Ala4	$< 2.6 \times 10^{-5}$	$> 2.7 \times 10^4$	2.5×10^3	$< 1.1 \times 10^{-8}$	> 10.9	Val81	−	−	5.1×10^2	−	−
Val5	$< 2.6 \times 10^{-5}$	$> 2.7 \times 10^4$	3.7×10^2	$< 7.0 \times 10^{-8}$	> 9.8	Gly82	$< 2.6 \times 10^{-5}$	$> 2.7 \times 10^4$	2.5×10^3	$< 1.0 \times 10^{-8}$	> 10.9
Ala6	−	−	5.6×10^3	−	−	Asp83	$< 2.6 \times 10^{-5}$	$> 2.7 \times 10^4$	1.3×10^4	$< 1.9 \times 10^{-9}$	> 11.9
Val7	$< 2.6 \times 10^{-5}$	$> 2.7 \times 10^4$	1.3×10^3	$< 2.0 \times 10^{-8}$	> 10.5	Leu84	$< 2.6 \times 10^{-5}$	$> 2.7 \times 10^4$	1.9×10^3	$< 1.3 \times 10^{-8}$	> 10.7
Leu8	$< 2.6 \times 10^{-5}$	$> 2.7 \times 10^4$	3.5×10^2	$< 7.3 \times 10^{-8}$	> 9.7	Gly85	−	−	2.1×10^3	−	−
Lys9	−	−	1.0×10^3	−	−	Asn86	1.5×10^{-2}	$4.6 \times 10^1 \pm 4 \times 10^0$	8.5×10^3	1.8×10^{-6}	7.8
Gly10	$> 2.8 \times 10^{-2}$	$< 2.5 \times 10$	4.6×10^3	$> 6.1 \times 10^{-6}$	< 7.1	Val87	$< 2.6 \times 10^{-5}$	$> 2.7 \times 10^4$	7.7×10^2	$< 3.4 \times 10^{-8}$	> 10.2
Asp11	$> 2.8 \times 10^{-2}$	$< 2.5 \times 10$	1.3×10^4	$> 2.1 \times 10^{-6}$	< 7.8	Thr88	$> 2.8 \times 10^{-2}$	$< 2.5 \times 10$	1.1×10^3	$> 2.4 \times 10^{-5}$	< 6.3
Gly12	$> 2.8 \times 10^{-2}$	$< 2.5 \times 10$	1.4×10^4	$> 2.0 \times 10^{-6}$	< 7.8	Ala89	$< 2.6 \times 10^{-5}$	$> 2.7 \times 10^4$	2.9×10^3	$< 8.8 \times 10^{-9}$	> 11.0
Pro13	−	−	2.7×10^3	−	−	Asp90	6.3×10^{-3}	$1.1 \times 10^2 \pm 4 \times 10^0$	9.1×10^3	6.9×10^{-7}	8.4
Val14	8.2×10^{-3}	$8.5 \times 10^1 \pm 3 \times 10^0$	1.5×10^3	5.5×10^{-6}	7.2	Lys91	−	−	6.7×10^3	−	−
Gln15	−	−	1.5×10^3	−	−	Asp92	$> 2.8 \times 10^{-2}$	$< 2.5 \times 10$	1.2×10^4	$> 2.3 \times 10^{-6}$	< 7.7
Gly16	−	−	5.5×10^3	−	−	Gly93	1.6×10^{-3}	$4.3 \times 10^2 \pm 3 \times 10$	1.4×10^4	1.2×10^{-7}	9.5
Val17	1.3×10^{-2}	$5.3 \times 10^1 \pm 4 \times 10^0$	5.1×10^2	2.6×10^{-5}	6.3	Val94	6.7×10^{-4}	$1.0 \times 10^3 \pm 2 \times 10$	5.5×10^2	1.2×10^{-6}	8.1
Ile18	$< 2.6 \times 10^{-5}$	$> 2.7 \times 10^4$	2.0×10^2	$< 1.3 \times 10^{-7}$	> 9.4	Ala95	1.1×10^{-4}	$(6.3 \pm 1) \times 10^3$	1.3×10^3	8.1×10^{-8}	9.7
Asn19	$< 2.6 \times 10^{-5}$	$> 2.7 \times 10^4$	3.4×10^3	$< 7.7 \times 10^{-9}$	> 11.1	Asp96	−	−	9.1×10^3	−	−
Phe20	−	−	2.2×10^3	−	−	Val97	$< 2.6 \times 10^{-5}$	$> 2.7 \times 10^4$	1.5×10^3	$< 1.8 \times 10^{-8}$	> 10.6
Glu21	$< 2.6 \times 10^{-5}$	$> 2.7 \times 10^4$	3.7×10^3	$< 7.0 \times 10^{-9}$	> 11.1	Ser98	−	−	3.2×10^3	−	−
Gln22	−	−	5.2×10^3	−	−	Ile99	1.2×10^{-4}	$(5.6 \pm 1) \times 10^3$	6.9×10^2	1.8×10^{-7}	9.2
Lys23	−	−	2.7×10^3	−	−	Glu100	$> 2.8 \times 10^{-2}$	$< 2.5 \times 10$	1.9×10^3	$> 1.5 \times 10^{-5}$	< 6.6
Glu24	−	−	4.3×10^3	−	−	Asp101	−	−	2.2×10^4	−	−
Ser25	−	−	1.1×10^4	−	−	Ser102	$> 2.8 \times 10^{-2}$	$< 2.5 \times 10$	1.7×10^4	$> 1.6 \times 10^{-6}$	< 7.9
Asn26	$> 2.8 \times 10^{-2}$	$< 2.5 \times 10$	1.1×10^4	$> 2.4 \times 10^{-6}$	< 7.7	Val103	−	−	7.4×10^2	−	−
Gly27	$> 2.8 \times 10^{-2}$	$< 2.5 \times 10$	7.2×10^3	$> 3.8 \times 10^{-6}$	< 7.4	Ile104	$< 2.6 \times 10^{-5}$	$> 2.7 \times 10^4$	2.5×10^2	$< 1.0 \times 10^{-7}$	> 9.5
Pro28	−	−	2.7×10^3	−	−	Ser105	$> 2.8 \times 10^{-2}$	$< 2.5 \times 10$	2.6×10^3	$> 1.1 \times 10^{-5}$	< 6.8
Val29	$< 2.6 \times 10^{-5}$	$> 2.7 \times 10^4$	1.5×10^3	$< 1.8 \times 10^{-8}$	> 10.6	Leu106	−	−	9.8×10^2	−	−
Lys30	−	−	1.2×10^3	−	−	Ser107	−	−	2.7×10^3	−	−
Val31	4.5×10^{-4}	$1.5 \times 10^3 \pm 2 \times 10^2$	4.9×10^2	9.3×10^{-7}	8.2	Gly108	−	−	6.9×10^3	−	−
Trp32	$< 2.6 \times 10^{-5}$	$> 2.7 \times 10^4$	5.2×10^2	$< 5.0 \times 10^{-8}$	> 10.0	Asp109	−	−	1.3×10^4	−	−
Gly33	2.5×10^{-4}	$2.8 \times 10^3 \pm 1 \times 10^2$	2.7×10^3	9.2×10^{-8}	9.6	His110	−	−	5.9×10^3	−	−
Ser34	8.7×10^{-3}	$7.9 \times 10^1 \pm 3 \times 10^0$	6.4×10^3	1.4×10^{-6}	8.0	Ser111	−	−	1.1×10^4	−	−
Ile35	$< 2.6 \times 10^{-5}$	$> 2.7 \times 10^4$	6.9×10^2	$< 3.8 \times 10^{-8}$	> 10.1	Ile112	−	−	1.2×10^3	−	−
Lys36	$> 2.8 \times 10^{-2}$	$< 2.5 \times 10$	1.0×10^3	$> 2.8 \times 10^{-5}$	< 6.2	Ile113	−	−	2.0×10^2	−	−
Gly37	1.8×10^{-2}	$3.8 \times 10^1 \pm 3 \times 10^0$	4.6×10^3	4.0×10^{-6}	7.4	Gly114	−	−	2.0×10^3	−	−
Leu38	$< 2.6 \times 10^{-5}$	$> 2.7 \times 10^4$	7.2×10^2	$< 3.6 \times 10^{-8}$	> 10.2	Arg115	−	−	3.3×10^3	−	−
Thr39	−	−	9.8×10^2	−	−	Thr116	$< 2.6 \times 10^{-5}$	$> 2.7 \times 10^4$	2.6×10^3	$< 9.9 \times 10^{-9}$	> 10.9
Glu40	$< 2.6 \times 10^{-5}$	$> 2.7 \times 10^4$	5.1×10^3	$< 5.1 \times 10^{-9}$	> 11.3	Leu117	$< 2.6 \times 10^{-5}$	$> 2.7 \times 10^4$	7.7×10^2	$< 3.4 \times 10^{-8}$	> 10.2
Gly41	−	−	8.5×10^3	−	−	Val118	$< 2.6 \times 10^{-5}$	$> 2.7 \times 10^4$	2.3×10^2	$< 1.1 \times 10^{-7}$	> 9.5
Leu42	−	−	7.2×10^2	−	−	Val119	$< 2.6 \times 10^{-5}$	$> 2.7 \times 10^4$	2.7×10^2	$< 9.7 \times 10^{-8}$	> 9.6
His43	−	−	9.1×10^2	−	−	His120	$< 2.6 \times 10^{-5}$	$> 2.7 \times 10^4$	1.1×10^3	$< 2.4 \times 10^{-8}$	> 10.4
Gly44	$< 2.6 \times 10^{-5}$	$> 2.7 \times 10^4$	4.8×10^3	$< 5.4 \times 10^{-9}$	> 11.3	Glu121	$< 2.6 \times 10^{-5}$	$> 2.7 \times 10^4$	4.5×10^3	$< 5.8 \times 10^{-9}$	> 11.2

Table 1. Continued

	k_{ex} (min^{-1})	$t_{1/2}$ (min)	k_{ch} (min^{-1})	K_{op}	ΔG_{op} (kcal mol^{-1} L^{-1})		k_{ex} (min^{-1})	$t_{1/2}$ (min)	k_{ch} (min^{-1})	K_{op}	ΔG_{op} (kcal mol^{-1} L^{-1})
Phe45	$<2.6\times10^{-5}$	$>2.7\times10^{4}$	1.6×10^{3}	$<1.6\times10^{-8}$	>10.6	Lys122	$<2.6\times10^{-5}$	$>2.7\times10^{4}$	4.2×10^{3}	$<6.3\times10^{-9}$	>11.2
His46	–	–	1.7×10^{3}	–	–	Ala123	–	–	2.5×10^{3}	–	–
Val47	$<2.6\times10^{-5}$	$>2.7\times10^{4}$	5.1×10^{2}	$<5.1\times10^{-8}$	>10.0	Asp124	$<2.6\times10^{-5}$	$>2.7\times10^{4}$	9.1×10^{3}	$<2.9\times10^{-9}$	>11.7
His48	$<2.6\times10^{-5}$	$>2.7\times10^{4}$	1.1×10^{3}	$<2.4\times10^{-8}$	>10.4	Asp125	6.6×10^{-5}	$1.0\times10^{4}\pm5\times10^{3}$	3.6×10^{4}	1.8×10^{-9}	11.9
Glu49	$<2.6\times10^{-5}$	$>2.7\times10^{4}$	4.5×10^{3}	$<5.8\times10^{-9}$	>11.2	Leu126	$<2.6\times10^{-5}$	$>2.7\times10^{4}$	1.9×10^{3}	$<1.3\times10^{-8}$	>10.7
Phe50	2.6×10^{-4}	$2.6\times10^{3}\pm1\times10^{1}$	2.6×10^{3}	1.0×10^{-7}	9.6	Gly127	1.5×10^{-4}	$(4.8\pm2)\times10^{3}$	2.1×10^{3}	6.8×10^{-8}	9.8
Gly51	4.6×10^{-4}	$1.5\times10^{3}\pm1\times10^{2}$	4.0×10^{3}	1.1×10^{-7}	9.5	Lys128	2.0×10^{-3}	$3.5\times10^{2}\pm9\times10^{0}$	2.5×10^{3}	7.9×10^{-7}	8.3
Asp52	2.9×10^{-4}	$2.4\times10^{3}\pm2\times10^{2}$	1.3×10^{4}	2.1×10^{-8}	10.5	Gly129	$>2.8\times10^{-2}$	$<2.5\times10$	4.6×10^{3}	$>6.1\times10^{-6}$	<7.1
Asn53	–	–	2.3×10^{4}	–	–	Gly130	$>2.8\times10^{-2}$	$<2.5\times10$	5.1×10^{3}	$>5.4\times10^{-6}$	<7.2
Thr54	1.1×10^{-2}	$6.5\times10^{1}\pm4\times10^{0}$	3.3×10^{3}	3.2×10^{-6}	7.5	Asn131	–	–	8.5×10^{3}	–	–
Ala55	$>2.8\times10^{-2}$	$<2.5\times10$	2.9×10^{3}	$>9.4\times10^{-6}$	<6.9	Glu132	$>2.8\times10^{-2}$	$<2.5\times10$	6.7×10^{3}	$>4.1\times10^{-6}$	<7.4
Gly56	$>2.8\times10^{-2}$	$<2.5\times10$	3.5×10^{3}	$>8.0\times10^{-6}$	<7.0	Glu133	$>2.8\times10^{-2}$	$<2.5\times10$	7.9×10^{3}	$>3.5\times10^{-6}$	<7.4
Cys57	$>2.8\times10^{-2}$	$<2.5\times10$	1.1×10^{4}	$>2.4\times10^{-6}$	<7.7	Ser134	–	–	1.1×10^{4}	–	–
Thr58	–	–	5.6×10^{3}	–	–	Thr135	$>2.8\times10^{-2}$	$<2.5\times10$	3.2×10^{3}	$>8.8\times10^{-6}$	<6.9
Ser59	–	–	6.9×10^{3}	–	–	Lys136	$>2.8\times10^{-2}$	$<2.5\times10$	2.7×10^{3}	$>1.0\times10^{-5}$	<6.8
Ala60	2.4×10^{-3}	$2.9\times10^{2}\pm5\times10^{0}$	3.7×10^{3}	6.4×10^{-7}	8.5	Thr137	$>2.8\times10^{-2}$	$<2.5\times10$	2.1×10^{3}	$>1.3\times10^{-5}$	<6.7
Gly61	$>2.8\times10^{-2}$	$<2.5\times10$	3.5×10^{3}	$>8.0\times10^{-6}$	<7.0	Gly138	1.7×10^{-3}	$4.0\times10^{2}\pm2\times10^{1}$	5.5×10^{3}	3.1×10^{-7}	8.9
Pro62	–	–	2.7×10^{3}	–	–	Asn139	3.1×10^{-3}	$2.2\times10^{2}\pm7\times10^{0}$	8.5×10^{3}	3.6×10^{-7}	8.8
His63	$>2.8\times10^{-2}$	$<2.5\times10$	5.9×10^{3}	$>4.7\times10^{-6}$	<7.3	Ala140	$>2.8\times10^{-2}$	$<2.5\times10$	3.9×10^{3}	$>7.1\times10^{-6}$	<7.0
Phe64	–	–	1.5×10^{3}	–	–	Gly141	$>2.8\times10^{-2}$	$<2.5\times10$	3.5×10^{3}	$>8.0\times10^{-6}$	<7.0
Asn65	$>2.8\times10^{-2}$	$<2.5\times10$	6.6×10^{3}	$>4.2\times10^{-6}$	<7.3	Ser142	$>2.8\times10^{-2}$	$<2.5\times10$	6.4×10^{3}	$>4.3\times10^{-6}$	<7.3
Pro66	–	–	3.9×10^{3}	–	–	Arg143	$>2.8\times10^{-2}$	$<2.5\times10$	4.5×10^{3}	$>6.2\times10^{-6}$	<7.1
Leu67	$>2.8\times10^{-2}$	$<2.5\times10$	2.8×10^{2}	$>9.9\times10^{-5}$	<5.5	Leu144	–	–	8.1×10^{2}	–	–
Ser68	–	–	2.7×10^{3}	–	–	Ala145	$<2.6\times10^{-5}$	$>2.7\times10^{4}$	1.1×10^{3}	$<2.3\times10^{-8}$	>10.4
Arg69	–	–	4.5×10^{3}	–	–	Cys146	1.3×10^{-3}	$5.2\times10^{2}\pm1\times10$	7.7×10^{3}	1.7×10^{-7}	9.2
Lys70	$>2.8\times10^{-2}$	$<2.5\times10$	2.8×10^{3}	$>9.8\times10^{-6}$	<6.8	Gly147	–	–	1.2×10^{4}	–	–
His71	7.3×10^{-5}	$(9.5\pm4)\times10^{3}$	1.9×10^{3}	3.8×10^{-8}	10.1	Val148	–	–	5.5×10^{2}	–	–
Gly72	$<2.6\times10^{-5}$	$>2.7\times10^{4}$	4.8×10^{3}	$<5.4\times10^{-9}$	>11.3	Ile149	–	–	2.5×10^{2}	–	–
Gly73	$<2.6\times10^{-5}$	$>2.7\times10^{4}$	5.1×10^{3}	$<5.1\times10^{-9}$	>11.3	Gly150	$<2.6\times10^{-5}$	$>2.7\times10^{4}$	2.0×10^{3}	$<1.3\times10^{-8}$	>10.8
Pro74	–	–	2.7×10^{3}	–	–	Ile151	2.7×10^{-4}	$2.5\times10^{3}\pm7\times10^{2}$	5.1×10^{2}	5.4×10^{-7}	8.6
Lys75	$>2.8\times10^{-2}$	$<2.5\times10$	9.8×10^{2}	$>2.8\times10^{-5}$	<6.2	Ala152	2.8×10^{-4}	$2.4\times10^{3}\pm4\times10^{2}$	1.1×10^{3}	2.6×10^{-7}	9.0
Asp76	$<2.6\times10^{-5}$	$>2.7\times10^{4}$	1.2×10^{4}	$<2.2\times10^{-9}$	>11.8	Gln153	–	–	2.1×10^{3}	–	–
Glu77	–	–	1.3×10^{4}	–	–						

[a]The positions at which the exchange could not be analyzed, due to signal overlap or severe line broadening, are indicated with dashes. The values of k_{ch} were taken from ref *44*.

Table 2: H−D Exchange Parameters for G93A[a]

	k_{ex} (min^{-1})	$t_{1/2}$ (min)	k_{ch} (min^{-1})	K_{op}	ΔG_{op} (kcal mol^{-1} L^{-1})		k_{ex} (min^{-1})	$t_{1/2}$ (min)	k_{ch} (min^{-1})	K_{op}	ΔG_{op} (kcal mol^{-1} L^{-1})
Ala1	−	−	1.9×10^3	−	−	Glu78	$> 2.8 \times 10^{-2}$	$< 2.5 \times 10$	7.9×10^3	$> 3.5 \times 10^{-6}$	< 7.4
Thr2	−	−	1.6×10^3	−	−	Arg79	6.9×10^{-4}	$1.0 \times 10^3 \pm 4 \times 10$	5.5×10^3	1.3×10^{-7}	9.4
Lys3	$> 2.8 \times 10^{-2}$	$< 2.5 \times 10$	2.7×10^3	$> 1.0 \times 10^{-5}$	< 6.8	His80	1.5×10^{-2}	$4.6 \times 10^1 \pm 2 \times 10^0$	2.5×10^3	6.1×10^{-6}	7.1
Ala4	$< 2.6 \times 10^{-5}$	$> 2.7 \times 10^4$	2.5×10^3	$< 1.1 \times 10^{-8}$	> 10.9	Val81	−	−	5.1×10^2	−;	−
Val5	$< 2.6 \times 10^{-5}$	$> 2.7 \times 10^4$	3.7×10^2	$< 7.0 \times 10^{-8}$	> 9.8	Gly82	$< 2.6 \times 10^{-5}$	$> 2.7 \times 10^4$	2.5×10^3	$< 1.0 \times 10^{-8}$	> 10.9
Ala6	−	−	5.6×10^3	−	−	Asp83	$< 2.6 \times 10^{-5}$	$> 2.7 \times 10^4$	1.3×10^4	$< 1.9 \times 10^{-9}$	> 11.9
Val7	$< 2.6 \times 10^{-5}$	$> 2.7 \times 10^4$	1.3×10^3	$< 2.0 \times 10^{-8}$	> 10.5	Leu84	$< 2.6 \times 10^{-5}$	$> 2.7 \times 10^4$	1.9×10^3	$< 1.3 \times 10^{-8}$	> 10.7
Leu8	$< 2.6 \times 10^{-5}$	$> 2.7 \times 10^4$	3.5×10^2	$< 7.3 \times 10^{-8}$	> 9.7	Gly85	−	−	2.1×10^3	−;	−
Lys9	−	−	1.0×10^3	−	−	Asn86	1.9×10^{-3}	$3.6 \times 10^2 \pm 1 \times 10^1$	8.5×10^3	2.3×10^{-7}	9.1
Gly10	$> 2.8 \times 10^{-2}$	$< 2.5 \times 10$	4.6×10^3	$> 6.1 \times 10^{-6}$	< 7.1	Val87	$< 2.6 \times 10^{-5}$	$> 2.7 \times 10^4$	7.7×10^2	$< 3.4 \times 10^{-8}$	> 10.2
Asp11	$> 2.8 \times 10^{-2}$	$< 2.5 \times 10$	1.3×10^4	$> 2.1 \times 10^{-6}$	< 7.8	Thr88	1.3×10^{-2}	$5.5 \times 10^1 \pm 2 \times 10^0$	1.1×10^3	1.1×10^{-5}	6.8
Gly12	$> 2.8 \times 10^{-2}$	$< 2.5 \times 10$	1.4×10^4	$> 2.0 \times 10^{-6}$	< 7.8	Ala89	1.0×10^{-4}	$(6.9 \pm 1) \times 10^3$	2.9×10^3	3.4×10^{-8}	10.2
Pro13	−	−	2.7×10^3	−	−	Asp90	$> 2.8 \times 10^{-2}$	$< 2.5 \times 10$	9.1×10^3	$> 3.0 \times 10^{-6}$	< 7.5
Val14	1.7×10^{-3}	$4.2 \times 10^2 \pm 3 \times 10^1$	1.5×10^3	1.1×10^{-6}	8.1	Lys91	−	−	6.7×10^3	−;	−
Gln15	−	−	1.5×10^3	−	−	Asp92	$> 2.8 \times 10^{-2}$	$< 2.5 \times 10$	1.2×10^4	$> 2.3 \times 10^{-6}$	< 7.7
Gly16	−	−	5.5×10^3	−	−	Gly93	−	−	7.4×10^3	−;	−
Val17	3.3×10^{-4}	$2.1 \times 10^3 \pm 5 \times 10^1$	5.1×10^2	6.4×10^{-7}	8.5	Val94	$> 2.8 \times 10^{-2}$	$< 2.5 \times 10$	3.7×10^2	$> 7.5 \times 10^{-5}$	< 5.6
Ile18	$< 2.6 \times 10^{-5}$	$> 2.7 \times 10^4$	2.0×10^2	$< 1.3 \times 10^{-7}$	> 9.4	Ala95	−	−	1.3×10^3	−;	
Asn19	$< 2.6 \times 10^{-5}$	$> 2.7 \times 10^4$	3.4×10^3	$< 7.7 \times 10^{-9}$	> 11.1	Asp96	$> 2.8 \times 10^{-2}$	$< 2.5 \times 10$	9.1×10^3	$> 3 \times 10^{-6}$	< 7.5
Phe20	−	−	2.2×10^3	−	−	Val97	$< 2.6 \times 10^{-5}$	$> 2.7 \times 10^4$	1.5×10^3	$< 1.8 \times 10^{-8}$	> 10.6
Glu21	$< 2.6 \times 10^{-5}$	$> 2.7 \times 10^4$	3.7×10^3	$< 7.0 \times 10^{-9}$	> 11.1	Ser98	−	−	3.2×10^3	−;	−
Gln22	−	−	5.2×10^3	−	−	Ile99	8.2×10^{-5}	$8.4 \times 10^3 \pm 1 \times 10^4$	6.9×10^2	1.2×10^{-7}	9.5
Lys23	−	−	2.7×10^3	−	−	Glu100	$> 2.8 \times 10^{-2}$	$< 2.5 \times 10$	1.9×10^3	$> 1.5 \times 10^{-5}$	< 6.6
Glu24	−	−	4.3×10^3	−	−	Asp101	−	−	2.2×10^4	−;	−
Ser25	−	−	1.1×10^4	−	−	Ser102	$> 2.8 \times 10^{-2}$	$< 2.5 \times 10$	1.7×10^4	$> 1.6 \times 10^{-6}$	< 7.9
Asn26	$> 2.8 \times 10^{-2}$	$< 2.5 \times 10$	1.1×10^4	$> 2.4 \times 10^{-6}$	< 7.7	Val103	−	−	7.4×10^2	−;	−
Gly27	1.4×10^{-2}	$4.8 \times 10^1 \pm 1 \times 10^0$	7.2×10^3	2.0×10^{-6}	7.8	Ile104	$< 2.6 \times 10^{-5}$	$> 2.7 \times 10^4$	2.5×10^2	$< 1.0 \times 10^{-7}$	> 9.5
Pro28	−	−	2.7×10^3	−	−	Ser105	$> 2.8 \times 10^{-2}$	$< 2.5 \times 10$	2.6×10^3	$> 1.1 \times 10^{-5}$	< 6.8
Val29	$< 2.6 \times 10^{-5}$	$> 2.7 \times 10^4$	1.5×10^3	$< 1.8 \times 10^{-8}$	10.6	Leu106	−	−	9.8×10^2	−;	−
Lys30	−	−	1.2×10^3	−	−	Ser107	−	−	2.7×10^3	−;	−
Val31	3.3×10^{-5}	$(2.1 \pm 4) \times 10^4$	4.9×10^2	6.8×10^{-8}	9.8	Gly108	−	−	6.9×10^3	−;	−
Trp32	$< 2.6 \times 10^{-5}$	$> 2.7 \times 10^4$	5.2×10^2	$< 5.0 \times 10^{-8}$	> 10.0	Asp109	−	−	1.3×10^4	−;	−
Gly33	6.3×10^{-4}	$1.1 \times 10^3 \pm 2 \times 10^1$	2.7×10^3	2.3×10^{-7}	9.1	His110	−	−	5.9×10^3	−;	−
Ser34	2.0×10^{-3}	$(3.5 \pm 2) \times 10^2$	6.4×10^3	3.1×10^{-7}	8.9	Ser111	−	−	1.1×10^4	−;	−
Ile35	$< 2.6 \times 10^{-5}$	$> 2.7 \times 10^4$	6.9×10^2	$< 3.8 \times 10^{-8}$	> 10.1	Ile112	−	−	1.2×10^3	−;	−
Lys36	−	−	1.0×10^3	−	−	Ile113	−	−	2.0×10^2	−;	−
Gly37	5.7×10^{-4}	$1.2 \times 10^3 \pm 3 \times 10^1$	4.6×10^3	1.3×10^{-7}	9.4	Gly114	−	−	2.0×10^3	−;	−
Leu38	−	−	7.2×10^2	−	−	Arg115	−	−	3.3×10^3	−;	−
Thr39	−	−	9.8×10^2	−	−	Thr116	$< 2.6 \times 10^{-5}$	$> 2.7 \times 10^4$	2.6×10^3	$< 9.9 \times 10^{-9}$	> 10.9
Glu40	$< 2.6 \times 10^{-5}$	$> 2.7 \times 10^4$	5.1×10^3	$< 5.1 \times 10^{-9}$	> 11.3	Leu117	$< 2.6 \times 10^{-5}$	$> 2.7 \times 10^4$	7.7×10^2	$< 3.4 \times 10^{-8}$	> 10.2
Gly41	−	−	8.5×10^3	−	−	Val117	$< 2.6 \times 10^{-5}$	$> 2.7 \times 10^4$	2.3×10^2	$< 1.1 \times 10^{-7}$	> 9.5
Leu42	−	−	7.2×10^2	−	−	Val119	3.8×10^{-4}	$1.8 \times 10^3 \pm 2 \times 10^2$	2.7×10^2	1.4×10^{-6}	8.0
His43	−	−	9.1×10^2	−	−	His120	$< 2.6 \times 10^{-5}$	$> 2.7 \times 10^4$	1.1×10^3	$< 2.4 \times 10^{-8}$	> 10.4
Gly44	$< 2.6 \times 10^{-5}$	$> 2.7 \times 10^4$	4.8×10^3	$< 5.4 \times 10^{-9}$	> 11.3	Glu121	$< 2.6 \times 10^{-5}$	$> 2.7 \times 10^4$	4.5×10^3	$< 5.8 \times 10^{-9}$	> 11.2

Table 2. Continued

	k_{ex} (min^{-1})	$t_{1/2}$ (min)	k_{ch} (min^{-1})	K_{op}	ΔG_{op} (kcal mol^{-1} L^{-1})		k_{ex} (min^{-1})	$t_{1/2}$ (min)	k_{ch} (min^{-1})	K_{op}	ΔG_{op} (kcal mol^{-1} L^{-1})
Phe45	$< 2.6 \times 10^{-5}$	$> 2.7 \times 10^{4}$	1.6×10^{3}	$< 1.6 \times 10^{-8}$	> 10.6	Lys122	$< 2.6 \times 10^{-5}$	$> 2.7 \times 10^{4}$	4.2×10^{3}	$< 6.3 \times 10^{-9}$	> 11.2
His46	–	–	1.7×10^{3}	–	–	Ala123	–	–	2.5×10^{3}	–;	–
Val47	3.3×10^{-5}	$(2.1 \pm 4) \times 10^{4}$	5.1×10^{2}	6.5×10^{-8}	9.8	Asp124	$< 2.6 \times 10^{-5}$	$> 2.7 \times 10^{4}$	9.1×10^{3}	$< 2.9 \times 10^{-9}$	> 11.7
His48	$< 2.6 \times 10^{-5}$	$> 2.7 \times 10^{4}$	1.1×10^{3}	$< 2.4 \times 10^{-8}$	> 10.4	Asp125	1.4×10^{-4}	$(5.0 \pm 1) \times 10^{3}$	3.6×10^{4}	3.9×10^{-9}	11.5
Glu49	3.0×10^{-3}	$2.3 \times 10^{2} \pm 1 \times 10^{1}$	4.5×10^{3}	6.8×10^{-7}	8.4	Leu126	$< 2.6 \times 10^{-5}$	$> 2.7 \times 10^{4}$	1.9×10^{3}	$< 1.3 \times 10^{-8}$	> 10.7
Phe50	2.3×10^{-2}	$3.0 \times 10^{1} \pm 3 \times 10^{0}$	2.6×10^{3}	8.7×10^{-6}	6.9	Gly127	1.7×10^{-4}	$4.1 \times 10^{3} \pm 6 \times 10^{2}$	2.1×10^{3}	8.0×10^{-8}	9.7
Gly51	3.4×10^{-4}	$2.0 \times 10^{3} \pm 1 \times 10^{2}$	4.0×10^{3}	8.6×10^{-8}	9.6	Lys128	2.6×10^{-5}	$(2.6 \pm 2) \times 10^{4}$	2.5×10^{3}	1.0×10^{-8}	10.9
Asp52	2.4×10^{-4}	$2.9 \times 10^{3} \pm 2 \times 10^{2}$	1.3×10^{4}	1.8×10^{-8}	10.6	Gly129	1.0×10^{-2}	$6.9 \times 10^{1} \pm 6 \times 10^{0}$	4.6×10^{3}	2.2×10^{-6}	7.7
Asn53	–	–	2.3×10^{4}	–	–	Gly130	$> 2.8 \times 10^{-2}$	$< 2.5 \times 10$	5.1×10^{3}	$> 5.4 \times 10^{-6}$	< 7.2
Thr54	2.7×10^{-3}	$2.6 \times 10^{2} \pm 5 \times 10^{0}$	3.3×10^{3}	8.1×10^{-7}	8.3	Asn131	–	–	8.5×10^{3}	–;	–
Ala55	2.3×10^{-2}	$3.0 \times 10^{1} \pm 2 \times 10^{0}$	2.9×10^{3}	7.7×10^{-6}	7.0	Glu132	$> 2.8 \times 10^{-2}$	$< 2.5 \times 10$	6.7×10^{3}	$> 4.1 \times 10^{-6}$	< 7.4
Gly56	$> 2.8 \times 10^{-2}$	$< 2.5 \times 10$	3.5×10^{3}	$> 8.0 \times 10^{-6}$	< 7.0	Glu133	$> 2.8 \times 10^{-2}$	$< 2.5 \times 10$	7.9×10^{3}	$> 3.5 \times 10^{-6}$	< 7.4
Cys57	$> 2.8 \times 10^{-2}$	$< 2.5 \times 10$	1.1×10^{4}	$> 2.4 \times 10^{-6}$	< 7.7	Ser134	–	–	1.1×10^{4}	–;	–
Thr58	–	–	5.6×10^{3}	–	–	Thr135	2.0×10^{-2}	$3.5 \times 10^{1} \pm 5 \times 10^{0}$	3.2×10^{3}	6.4×10^{-6}	7.1
Ser59	–	–	6.9×10^{3}	–	–	Lys136	4.6×10^{-3}	$1.5 \times 10^{2} \pm 6 \times 10^{0}$	2.7×10^{3}	1.7×10^{-6}	7.9
Ala60	1.3×10^{-4}	$5.4 \times 10^{3} \pm 5 \times 10^{2}$	3.7×10^{3}	3.4×10^{-8}	10.2	Thr137	$> 2.8 \times 10^{-2}$	$< 2.5 \times 10$	2.1×10^{3}	$> 1.3 \times 10^{-5}$	< 6.7
Gly61	7.8×10^{-3}	$8.9 \times 10^{1} \pm 5 \times 10^{0}$	3.5×10^{3}	2.3×10^{-6}	7.7	Gly138	$< 2.6 \times 10^{-5}$	$> 2.7 \times 10^{4}$	5.5×10^{3}	$< 4.7 \times 10^{-9}$	> 11.4
Pro62	–	–	2.7×10^{3}	–	–	Asn139	$> 2.8 \times 10^{-2}$	$< 2.5 \times 10$	8.5×10^{3}	$> 3.3 \times 10^{-6}$	< 7.5
His63	$> 2.8 \times 10^{-2}$	$< 2.5 \times 10$	5.9×10^{3}	$> 4.7 \times 10^{-6}$	< 7.3	Ala140	$> 2.8 \times 10^{-2}$	$< 2.5 \times 10$	3.9×10^{3}	$> 7.1 \times 10^{-6}$	< 7.0
Phe64	–	–	1.5×10^{3}	–	–	Gly141	$> 2.8 \times 10^{-2}$	$< 2.5 \times 10$	3.5×10^{3}	$> 8.0 \times 10^{-6}$	< 7.0
Asn65	$> 2.8 \times 10^{-2}$	$< 2.5 \times 10$	6.6×10^{3}	$> 4.2 \times 10^{-6}$	< 7.3	Ser142	$> 2.8 \times 10^{-2}$	$< 2.5 \times 10$	6.4×10^{3}	$> 4.3 \times 10^{-6}$	< 7.3
Pro66	–	–	3.9×10^{3}	–	–	Arg143	$> 2.8 \times 10^{-2}$	$< 2.5 \times 10$	4.5×10^{3}	$> 6.2 \times 10^{-6}$	< 7.1
Leu67	2.4×10^{-3}	$2.9 \times 10^{2} \pm 5 \times 10^{0}$	2.8×10^{2}	8.5×10^{-6}	6.9	Leu144	–	–	8.1×10^{2}	–;	–
Ser68	–	–	2.7×10^{3}	–	–	Ala145	$< 2.6 \times 10^{-5}$	$> 2.7 \times 10^{4}$	1.1×10^{3}	$< 2.3 \times 10^{-8}$	> 10.4
Arg69	–	–	4.5×10^{3}	–	–	Cys146	–	–	7.7×10^{3}	–;	–
Lys70	$> 2.8 \times 10^{-2}$	$< 2.5 \times 10$	2.8×10^{3}	$> 9.8 \times 10^{-6}$	< 6.8	Gly147	–	–	1.2×10^{4}	–;	–
His71	2.4×10^{-4}	$2.9 \times 10^{3} \pm 2 \times 10^{2}$	1.9×10^{3}	1.2×10^{-7}	9.4	Val148	–	–	5.5×10^{2}	–;	–
Gly72	$> 2.8 \times 10^{-2}$	$< 2.5 \times 10$	4.8×10^{3}	$> 5.8 \times 10^{-6}$	< 7.1	Ile149	–	–	2.5×10^{2}	–;	–
Gly73	$< 2.6 \times 10^{-5}$	$> 2.7 \times 10^{4}$	5.1×10^{3}	$< 5.1 \times 10^{-9}$	> 11.3	Gly150	$< 2.6 \times 10^{-5}$	$> 2.7 \times 10^{4}$	2.0×10^{3}	$< 1.3 \times 10^{-8}$	> 10.8
Pro74	–	–	2.7×10^{3}	–	–	Ile151	–	–	5.1×10^{2}	–;	–
Lys75	$> 2.8 \times 10^{-2}$	$< 2.5 \times 10$	9.8×10^{2}	$> 2.8 \times 10^{-5}$	< 6.2	Ala152	1.5×10^{-4}	$(4.7 \pm 3) \times 10^{3}$	1.1×10^{3}	1.3×10^{-7}	9.4
Asp76	2.7×10^{-3}	$2.5 \times 10^{2} \pm 5 \times 10^{0}$	1.2×10^{4}	2.3×10^{-7}	9.1	Gln153	–	–	2.1×10^{3}	–;	–
Glu77	–	–	1.3×10^{4}	–	–						

[a] The positions at which the exchange could not be analyzed, due to signal overlap or severe line broadening, are indicated with dashes. The values of k_{ch} were taken from ref *44*.

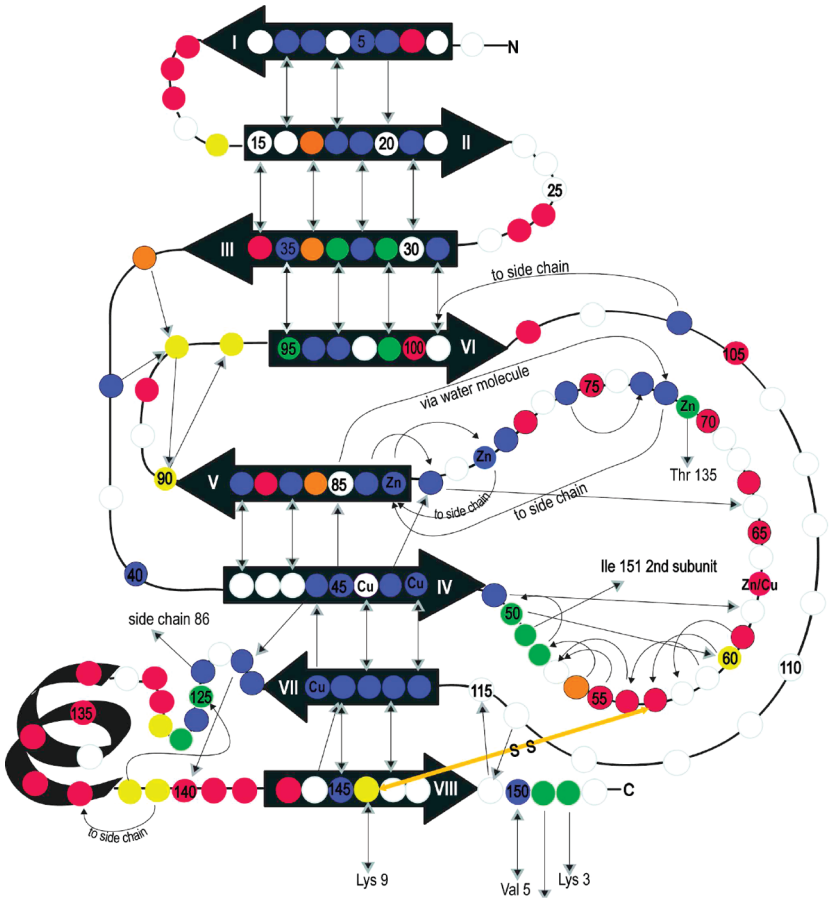

FIGURE 1: Schematic drawing of the subunit showing the exchange pattern for wt CuZnSOD. Amino acids for which the H−D exchange is too slow to be detected during the chosen period ($t_{1/2}$ > 18 days) are colored blue. Amide protons with quantifiable (up to ~18 days) half-lives longer than 1 day (1 day < $t_{1/2}$ < 18 days) are colored green. H−D exchange with half-lives between 1 h and 1 day are colored yellow. Amide protons with fast H−D exchange rates (25 min < $t_{1/2}$ < 1 h) are colored orange, and amide protons that were fully exchanged even before the first measurement ($t_{1/2}$ < 25 min) are colored red. Amino acids that are not assigned (prolines included) due to overlap and weak or missing peaks are colored white. Copper and zinc binding sites are labeled with Cu and Zn, respectively. The black numbered arrows illustrate the eight β-sheets, and the gray arrows between the amino acids indicate hydrogen bonds in the secondary structure as determined by the crystal structure (PDB entry 2C9V) pointing from H to O.

Loops 1 and 2 are positioned with a high degree of surface exposure with no stabilizing hydrogen bond and accordingly exhibited rapid exchange.

In loop 3, the amide protons of Gly37 and Leu38 both form hydrogen bonds to Gly93. However, their exchange rates differed considerably: Gly37 exchanged rather fast ($t_{1/2}$ = 38 min), and Leu38 had an exchange rate that was much lower ($t_{1/2}$ > 18 days). Surprisingly, the exchange of Glu40 was very slow ($t_{1/2}$ > 18 days), which was unexpected since there is no identified stabilizing hydrogen bond for Glu40. An explanation could be that the amide proton of Glu40 forms a hydrogen bond with the acid group from its own side chain.

Loop 4, also called the zinc binding loop, contains elements with different stability. The first part of the loop (Glu49−Asp52) exhibited slow exchange. Glu49 demonstrated no measurable exchange, and the $t_{1/2}$ values for Phe50, Gly51, and Asp52 were 1.8, 1.1, and 1.7 days, respectively. In this part of the loop, all backbone amide protons are involved in hydrogen bonds (Glu49 to Pro62, Phe50 to Ala60, and Gly51 to Ile151 in the second subunit and Asp52 to Phe50). The second part of loop 4 (Thr54−Lys70) exhibited very fast exchange. With the exception of Ala60, all amide protons between Ala55 and Lys70 were fully exchanged in < 1 h. The last part of loop 4 encloses two of the four zinc ligands, His71 and His80. This part showed a mixed exchange pattern. Lys75 and Glu78 were fully exchanged within the dead time of the experiment, and His71 has a $t_{1/2}$ of 6.5 days. The remaining residues (Gly72, Gly73, Asp76, Arg79, His80, and Gly82) exhibited very slow exchange, and with the exception of Gly73 and Arg79, they are stabilized by identified hydrogen bonds.

Within loop 5, the amide proton of Asp90 hydrogen bonds to the backbone carbonyl of Val94. The amide proton of Val94 forms a hydrogen bond to the side chain of Asp90, and the Gly93 amide proton binds to the backbone carbonyl of Asp90. Those residues all had exchange rates in the range of 2−18 h. Asp92, on the other hand, was fully exchanged in < 1 h.

Unfortunately, only three of the 13 amide protons in loop 6 could be observed. The resonance in this area was either very weak and/or broad or completely absent. Apparently, this loop has an internal dynamics that gives rise to multiple conformations with lifetimes that may cause severe line broadening.

Loop 7 which is called the electrostatic loop is located close to the active site. In the first part (residues 121−126), all residues are stabilized by identified hydrogen bonds (121 → 142 and 142 → 121 side chain, 122 → 140, 124 → 86 side chain, 125 → 138 and 126 → 124; some of them are not shown in Figure 1) and those residues exhibited slow exchange. In the remaining part

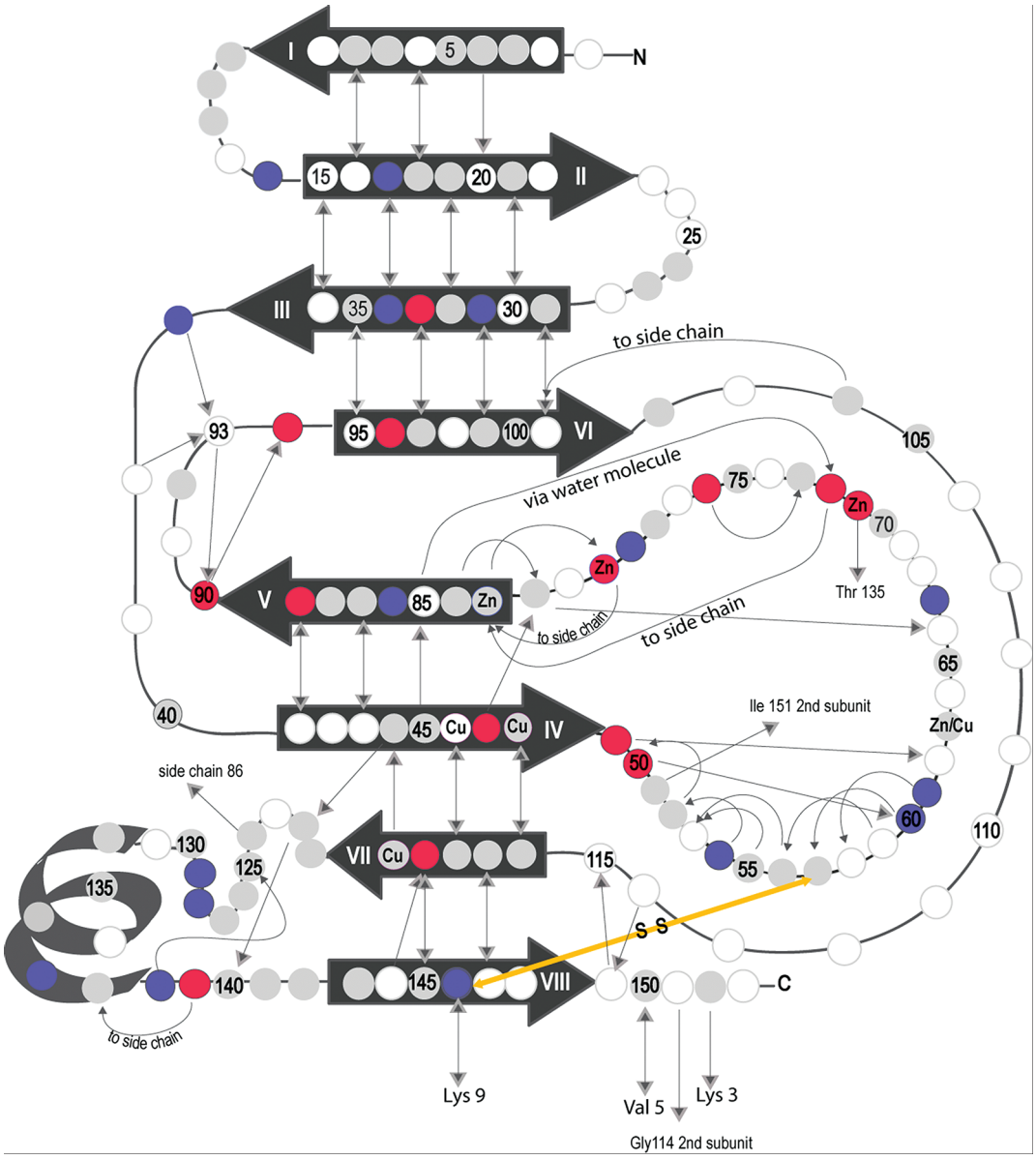

FIGURE 2: Schematic of the subunit showing the differences in exchange patterns for G93A compared to wt CuZnSOD. Amino acids that are destabilized in G93A ($\Delta G_{wt} - \Delta G_{G93A} \geq -0.5$ kcal/mol) are colored red. Amide protons that are stabilized in G93A ($\Delta G_{wt} - \Delta G_{G93A} \geq 0.5$ kcal/mol) are colored blue. Amino acids for which the H−D exchange rate was similar in wt CuZnSOD and G93A are colored gray. Amino acids that are not assigned (prolines included) due to overlap and weak or missing peaks are colored white. Copper and zinc binding sites are labeled with Cu and Zn, respectively. The G93A mutation is colored pink. The black numbered arrows illustrate the eight β-sheets, and the gray arrows between the amino acids indicate hydrogen bonds in the secondary structure as determined by the crystal structure (PDB entry 2C9V) pointing in the direction from H to O.

(comprising a 3^{10}-helix), the exchange was very fast where most of the amide protons were completely exchanged in <1 h. Thus, this helical structure seems to be flexible.

Loop 8 contains the last five amino acids. We were able to detect exchange for three of them: Gly150, Ile151, and Ala152. All exhibited slow exchange ($t_{1/2} > 18$ days, $t_{1/2} = 1.8$ days, and $t_{1/2} = 1.7$ days, respectively) which can be explained by their hydrogen bonds to Val5, Gly114 from the second subunit, and Lys3, respectively.

Exchange Patterns for G93A. All the results for G93A are listed in Table 2. The measurement with G93A showed that 29 of the investigated (observable) backbone NH resonances were fully exchanged within the dead time of the experiment; i.e., the original signal had disappeared before completion of the first spectrum ($t_{1/2} < 25$ min). For 34 resonances, it was possible to determine the exchange rate. For five of these resonances, the half-lives were between 25 min and 1 h, 14 protons exchanged with half-lives between 1 h and 1 day, and 14 protons exchanged with half-lives between 1 and 18 days. For 33 amide protons, the exchange was too slow to measure.

Comparison of G93A with wt CuZnSOD. The difference in the exchange pattern for G93A compared to that of wt CuZnSOD is summarized in Figure 2. For 65 amide protons, similar exchange rates ($\Delta G_{wt} - \Delta G_{G93A} < \pm 0.5$ kcal/mol) were found in G93A and wt CuZnSOD. Fourteen amide protons exchanged faster (destabilization) and 16 amide protons slower (stabilization) in G93A compared to wt CuZnSOD.

(*i*) *The Area in the Vicinity of the Mutation Site Is Destabilized in G93A*. Residues Ala89, Asp90, Val94, and Asp96, enclosing the mutated site G93A, have been destabilized where the amide proton of Asp90, Val94, and Asp96 were fully exchanged in <1 h. Interestingly, residue 33 in the neighboring

β-strand III, which donates a hydrogen bond to residue 97, was also slightly destabilized.

(*ii*) *The G93A Mutation Causes Stabilization of the β-Strand II−β-Strand III Hairpin and at Scattered Positions*. The open end of the of the β-strand II−β-strand III hairpin is stabilized by the G93A mutation as evidenced by the reduced exchange rates for the hydrogen bond pair, Val17 (β-strand II)−Ser34 (β-strand III), and for residues Val14 and Gly37. Notably, this region is situated close to the mutation site. As shown by blue-colored residues in Figure 2, there are also several positions that are stabilized at positions that are distributed over the entire structure with no obvious pattern of internal connections.

(*iii*) *The Area in the Vicinity of the Metal Binding Site Is Destabilized in G93A*. Besides the distinct enhancement of the H−D exchange rate for NH protons in the vicinity of the mutation site, nine additional NH protons experienced a pronounced increase in H−D exchange rate in G93A compared to wt CuZnSOD (Val47, Glu49, Phe50, His71, Gly72, Asp76, His80, Val119, and Asp139). Interestingly, these amino acids are positioned in a bonding network that includes the metal binding ligands (Figure 2). Six of these destabilized NH protons (Val47, Glu49, Gly72, Asp76, His80, and Val119) demonstrated very slow H−D exchange rates ($t_{1/2}$ > 18 days) in the wt CuZnSOD protein. In G93A, the H−D exchange of Val47 and Val119 was still quite slow ($t_{1/2}$ = 14.5 and 1.3 days, respectively), but for the remainder, the rate was increased pronouncedly with half-lives on the order of hours and minutes (3.8 h for Glu49, < 25 min for Gly72, 4.2 h for Asp76, and 46 min for His80). In wt CuZnSOD, Phe50 and Asp139 had rather short half-lives (1.8 days and 3.7 h, respectively), but both exhibited even faster exchange in G93A (1.8 h and < 25 min, respectively). According to the crystal structure, with the exception of Asp139, this group of backbone NH resonances all participate in hydrogen bonds around the Zn and Cu sites (Val47 → Gly82, Glu49 → Pro62, Phe50 → Ala60, His71 → Thr135, Gly72 → side chain in Asp83, Asp76 → Gly73, His80 → side chain in Asp83, and Val119 → Ala145). These findings will be discussed in detail in the Discussion.

(*iv*) *Effects on the Dimer Interface*. Among the residues that are involved in the dimer interface, it was possible to observe hydrogen exchange for five residues. Four of these (Gly51, Asp52, Gly150, and Ala152) were not affected by the mutation. Notably, Phe50 which is closely connected to the metal binding ligands was the only destabilized residue in the interface.

DISCUSSION

In this section, we will highlight the effect of the G93A mutation on the local dynamics and stability and discuss possible consequences for the aggregation mechanism.

wt CuZnSOD is characterized by a very high conformational stability (*25*). The result from this study does indeed show that the core of wt CuZnSOD is very stable. After H−D exchange for 4.5 days, half (50 peaks) of the studied (nonoverlapping) amide protons were still visible in the 2D ^{15}N−^{1}H HSQC spectrum and 39 of these NH protons exhibited no reduction at all in their peak intensity.

Destabilization at the G93A Mutation Site. The structure in the vicinity of the mutation site is markedly destabilized. The destabilized region encompasses amino acids 89−96 which are shown by the destabilization at residues Ala89, Asp90, Val94, and Asp96 (Figures 2 and 3). Interestingly, the G93A mutation causes destabilization in two distinct regions only, the region surrounding the mutation and the metal binding region discussed below. In addition, the mutation does also cause a marked stabilization at several positions that are more scattered in the structure. Analysis of the H−D exchange at the β-strand II−β-strand III hairpin showed that this hairpin is considerably flexible in the wt protein (Figure 1). Interestingly, this hairpin is markedly stabilized in the G93A protein (Figure 2). Apparently, the G93A mutation is causing a destabilization at the mutation site which allows this neighboring hairpin region to find a more energetically advantageous conformation. Considering that the Gly to Ala mutation, which reduces the degree of conformational freedom in loop 3, is causing a destabilization in this area, it is remarkable to find that the neighboring β-hairpin is stabilized (Figure 3). One intriguing possibility is that the destabilization of the hydrogen bond between residue 33 in strand III and residue 97 in strand IV allows small conformational adjustments of the β-strand II−β-strand III hairpin resulting in increased stability.

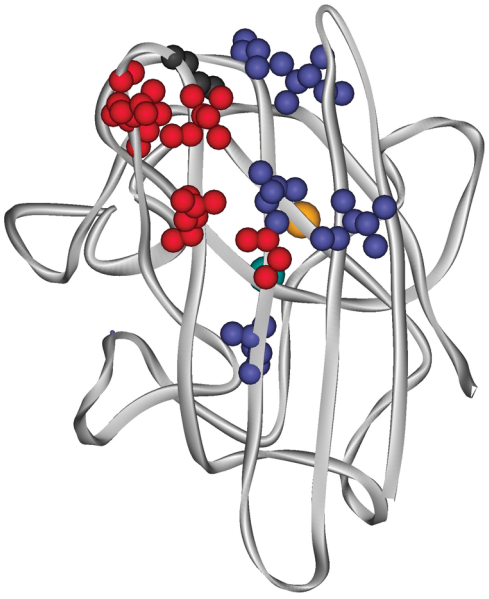

FIGURE 3: Destabilized amino acids located at the G93A mutation site are colored red. Stabilized amino acids located in the β-strand II−β-strand III hairpin of G93A are colored blue. The copper ion is colored light blue, and the zinc ion is colored yellow. The G93A mutation site is colored black.

The remaining stabilized amino acids appear at scattered positions over the entire molecule. Notably, it seems as if most of the stabilized residues are situated close to the surface of the molecule (Figure 4)

Destabilization of a Discrete Structural Element Surrounding the Metal Binding Sites. In addition to the destabilization of the hydrogen bond network found around the mutation site, nine additional residues exhibited an enhanced rate of H−D exchange in G93A compared to that in wt. All of them are positioned in the surrounding area of the zinc and the copper site (Figure 5). Especially Glu49, Phe50, Gly72, Asp76, His80, and Val119 were highly destabilized ($\Delta\Delta G_{wt-G93A}$ > 1.6 kcal/mol) in G93A compared to wt (Figure 6). Notably, an extreme destabilization ($\Delta\Delta G_{wt-G93A}$ > 4 kcal/mol) is found for Gly72 (His71 is a zinc ligand) and His80 (zinc ligand). It is apparent that the destabilization, which is caused by the G93A mutation, is limited to a distinct region in SOD, i.e., the metal binding region. The H−D exchange experiments were performed

with concentrations of both protein monomers and metal ions of approximately 0.5 mM. Therefore, the results cannot be used to calculate differences in metal binding affinities, which are several orders of magnitude higher. Since the metal binding region in G93A has increased dynamics compared to that of wt SOD, it is reasonable to assume that the metal affinity is lowered in the G93A variant; i.e., the chelate effect may be weaker in G93A.

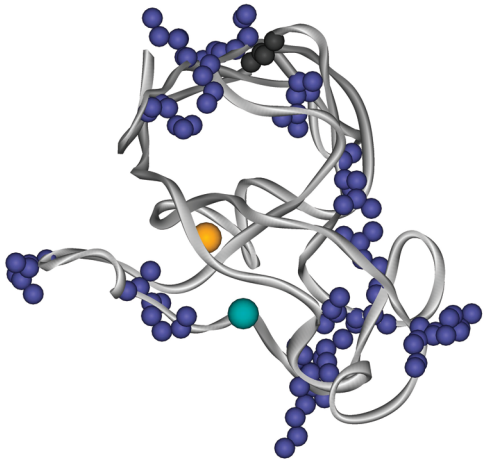

FIGURE 4: Amino acids that are stabilized in G93A are colored blue. The copper ion is colored light blue, and the zinc ion is colored yellow. The G93A mutation site is colored black.

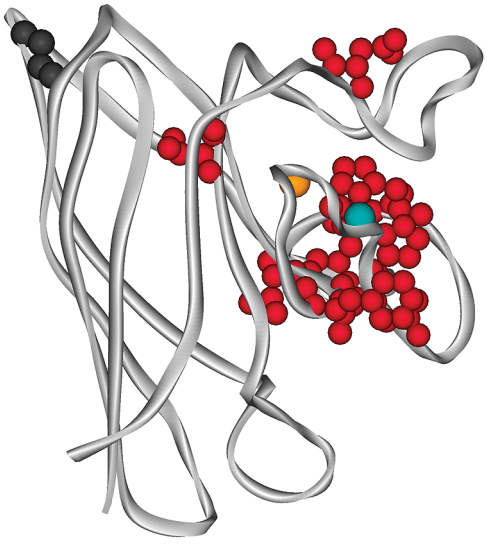

FIGURE 5: All destabilized amino acids (red) remote from the mutation site (black) are positioned in the surrounding area of the zinc and copper site. The copper ion is colored light blue, and the zinc ion is colored yellow.

Linking Destabilization at the Mutation Site with Destabilization at the Distinct Metal Binding Region. In small proteins, the effect of a mutation is often manifested in a global destabilization of the entire protein, a result that is ascribed to a tight cooperative coupling involving all parts of the protein. In SOD, we observe that the G93A mutation selectively destabilizes two distinct regions of the protein. This result shows that SOD is not stabilized as a single cooperative unit. Instead, the stability or dynamics of distinct subregions is closely coupled without notable effects on other regions. Apparently, the region around G93 is cooperatively coupled to the rather distant metal binding region. This effect is similar to that which is found in many allosterically regulated or signal transducing proteins. The apparent question is what constitutes the physical links that transmit the information from the mutation site at G93 to the metal binding region. An inspection of the SOD structure shows that the most direct link between the sites is β-strand V, which is a surface-exposed edge strand of a four-stranded β-sheet (Figure 7). Inspection of H−D exchange for residues in this strand shows a significant difference for only residue Asn86 which is slightly stabilized in the mutated protein. The results from this study and the results from the study by Shipp et al. (*41*) also show that the shifts for the NH protons in this strand are very similar in the wt and G93A proteins except for minor shift differences of 0.05 ppm at positions 87 and 89. These results indicate that very small alterations in this strand are sufficient to cause large effects in the dynamics of the metal binding region.

Effects on the Dimer Interface. Effects of the ALS mutation on the stability of the dimer interface have been extensively discussed (*47*). For example, a H−D study by Shaw et al. (*38*) showed differences in the exchange pattern for a peptide comprising amino acids Phe50, Gly51, Asp52, and Asn53, indicating a destabilized dimer interface in apo A4V. For that mutant, they found an increase in the rate of H−D exchange corresponding to the exchange of two more protons compared to apo wt CuZnSOD. In our study on the holoproteins, the backbone amide proton of residue Phe50 is the only amino acid residue in the dimer interface that is destabilized. This residue is as noted above also part of the destabilized metal binding region. Thus, the destabilization of the metal binding region seems to have small effects on the stability of the major part of the dimer interface despite the obvious connection via Phe50; i.e., no differences between wt CuZnSOD and G93A in the exchange pattern are observed for residues Gly51, Asp52, Gly150, and Ala152 comprising a major part of the dimer interface. However, it should be

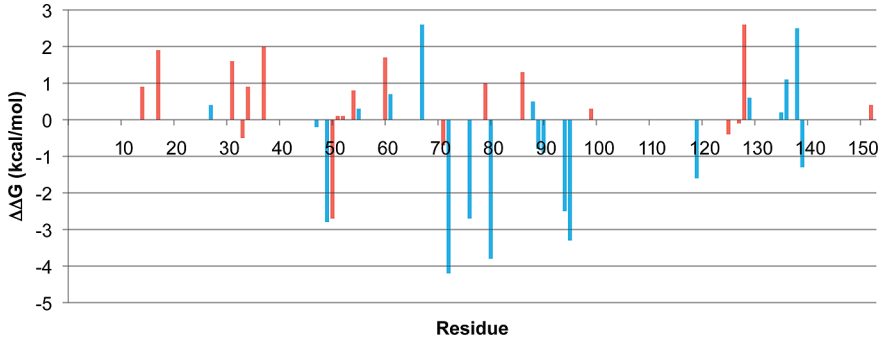

FIGURE 6: Differences in stability between wt CuZnSOD and G93A ($\Delta\Delta G_{wt-G93A}$). Negative values indicate destabilization by the G93A mutation. Red bars indicate exact measured differences, while blue bars denote a lower limit for the difference.

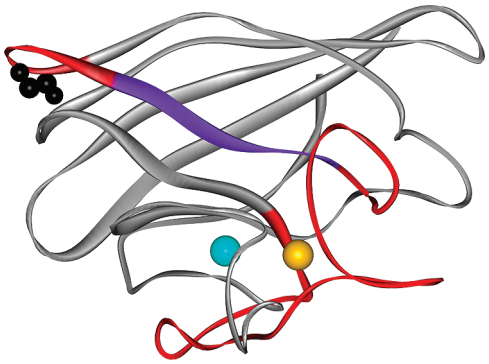

FIGURE 7: Destabilization in the surrounding area (red) of the zinc (yellow) and copper (light blue) site might be mediated by a small disruption in the neighboring β-strand V (purple) as a consequence of the destabilization in the loop structure (red) comprising the G93A mutation (black) which is connected to β-strand V.

noted that although the results indicate that the dimer interface is remarkably stable in both holo wt CuZnSOD and the holo G93A variant, the results do not exclude the possibility that the G93A mutation reduces the dimer affinity significantly from a highly stable state in holo wt CuZnSOD.

Internal Mobility. The structural and dynamic properties of pseudo wt CuZnSOD and a pseudo G93A variant have been compared in a thorough NMR study by Banci et al. (*42*) and Shipp et al. (*41*). In their studies, differences in internal mobility between the two variants of SOD are estimated from measurements of relaxation rates which were analyzed in a model-free approach giving so-called order parameters. These order parameters report on the mobility of backbone NH resonances on the picosecond to millisecond time scale. In our study, the H−D exchange rates report on mobility on a time scale from minutes to days. The comparison at all measured positions shows no obvious correlations between these parameters, nor do we find a correlation in any of the most affected regions (the mutation site and the metal binding site). Thus, it seems as if the rather large scale movements, which are required for H−D exchange, are not affected by the fast and small scale alterations at the N−H vector that is reported by the model free order parameters. The comparison also indicates that the G93A mutation results in an increased small scale dynamics at a majority of NH positions in the protein, while H−D exchange reports that increase in the large scale dynamics is restricted and occurs in two well-defined regions only.

CONCLUSIONS

Apparently, the G93A mutation selectively destabilizes the metal binding region which is remote from the site of mutation. The result may indicate that the metal binding region, in its fully metalated state, can become prone to participation in intermolecular protein−protein interactions leading to formation of aggregates.

The selective destabilization of the metal binding region in combination with the maintained stability of the dimer interface indicates that the G93A variant can participate in aggregation in its dimeric form; i.e., formation of monomeric species may not be an obligatory step in the elongation of SOD fibrils, in contrast to the suggestions by Rakhit et al. (*48*). Instead, the results seem to reinforce the recent results of Chattopadhyay et al. (*40*) which show that once SOD fibrillation is initiated, the fibrils can grow by addition of relatively nativelike forms of SOD.

Notably, the study by Ermilova et al. (*49*) of transgenic G93A mice shows that a well-balanced addition of Zn and of a Zn/Cu mixture can protect against the toxicity of the ALS-associated SOD mutant, also pointing to the importance of the metal binding region in the pathogenesis of ALS.

SUPPORTING INFORMATION AVAILABLE

Theory behind the H−D exchange experiments. This material is available free of charge via the Internet at http://pubs.acs.org.

REFERENCES

1. Soto, C. (2003) Unfolding the role of protein misfolding in neurodegenerative diseases. *Nat. Rev. Neurosci. 4*, 49–60.
2. Adams, R. D., Vinctor, M., and Ropper, A. H. (1998) *Principles of Neurology*, McGraw-Hill Health Professions Division, New York.
3. Orrell, R. W., Habgood, J. J., Gardiner, I., King, A. W., Bowe, F. A., Hallewell, R. A., Marklund, S. L., Greenwood, J., Lane, R. J. M., and deBelleroche, J. (1997) Clinical and functional investigation of 10 missense mutations and a novel frameshift insertion mutation of the gene for copper-zinc superoxide dismutase in UK families with amyotrophic lateral sclerosis. *Neurology 48*, 746–751.
4. Rosen, D. R., Siddique, T., Patterson, D., Figlewicz, D. A., Sapp, P., Hentati, A., Donaldson, D., Goto, J., O'Regan, J. P., and Deng, H. X.; et al. (1993) Mutations in Cu/Zn superoxide dismutase gene are associated with familial amyotrophic lateral sclerosis. *Nature 362*, 59–62.
5. Deng, H. X., Hentati, A., Tainer, J. A., Iqbal, Z., Cayabyab, A., Hung, W. Y., Getzoff, E. D., Hu, P., Herzfeldt, B., and Roos, R. P. et al. (1993) Amyotrophic lateral sclerosis and structural defects in Cu,Zn superoxide dismutase. *Science 261*, 1047–1051.
6. Elshafey, A., Lanyon, W. G., and Connor, J. M. (1994) Identification of a New Missense Point Mutation in Exon-4 of the Cu/Zn Superoxide-Dismutase (Sod-1) Gene in a Family with Amyotrophic-Lateral-Sclerosis. *Hum. Mol. Genet. 3*, 363–364.
7. Guegan, C., and Przedborski, S. (2003) Programmed cell death in amyotrophic lateral sclerosis. *J. Clin. Invest. 111*, 153–161.
8. Borchelt, D. R., Lee, M. K., Slunt, H. S., Guarnieri, M., Xu, Z. S., Wong, P. C., Brown, R. H., Price, D. L., Sisodia, S. S., and Cleveland, D. W. (1994) Superoxide-Dismutase-1 with Mutations Linked to Familial Amyotrophic-Lateral-Sclerosis Possesses Significant Activity. *Proc. Natl. Acad. Sci. U.S.A. 91*, 8292–8296.
9. Gurney, M. E., Pu, H. F., Chiu, A. Y., Dalcanto, M. C., Polchow, C. Y., Alexander, D. D., Caliendo, J., Hentati, A., Kwon, Y. W., Deng, H. X., Chen, W. J., Zhai, P., Sufit, R. L., and Siddique, T. (1994) Motor-Neuron Degeneration in Mice That Express a Human Cu,Zn Superoxide-Dismutase Mutation. *Science 264*, 1772–1775.
10. Reaume, A. G., Elliott, J. L., Hoffman, E. K., Kowall, N. W., Ferrante, R. J., Siwek, D. F., Wilcox, H. M., Flood, D. G., Beal, M. F., Brown, R. H., Scott, R. W., and Snider, W. D. (1996) Motor neurons in Cu/Zn superoxide dismutase-deficient mice develop normally but exhibit enhanced cell death after axonal injury. *Nat. Genet. 13*, 43–47.
11. Shinder, G. A., Lacourse, M. C., Minotti, S., and Durham, H. D. (2001) Mutant Cu/Zn-superoxide dismutase proteins have altered solubility and interact with heat shock/stress proteins in models of amyotrophic lateral sclerosis. *J. Biol. Chem. 276*, 12791–12796.
12. Okado-Matsumoto, A., and Fridovich, I. (2002) Amyotrophic lateral sclerosis: A proposed mechanism. *Proc. Natl. Acad. Sci. U.S.A. 99*, 9010–9014.
13. Rousseau, F., Schymkowitz, J., and Oliveberg, M. (2008) ALS precursor finally shaken into fibrils. *Proc. Natl. Acad. Sci. U.S.A. 105*, 18649–18650.
14. Durham, H. D., Roy, J., Dong, L., and Figlewicz, D. A. (1997) Aggregation of mutant Cu/Zn superoxide dismutase proteins in a culture model of ALS. *J. Neuropathol. Exp. Neurol. 56*, 523–530.
15. Bruijn, L. I., Houseweart, M. K., Kato, S., Anderson, K. L., Anderson, S. D., Ohama, E., Reaume, A. G., Scott, R. W., and Cleveland, D. W. (1998) Aggregation and motor neuron toxicity of an ALS-linked SOD1 mutant independent from wild-type SOD1. *Science 281*, 1851–1854.
16. Johnston, J. A., Dalton, M. J., Gurney, M. E., and Kopito, R. R. (2000) Formation of high molecular weight complexes of mutant Cu,Zn-superoxide dismutase in a mouse model for familial amyotrophic lateral sclerosis. *Proc. Natl. Acad. Sci. U.S.A. 97*, 12571–12576.

17. Stieber, A., Gonatas, J. O., and Gonatas, N. K. (2000) Aggregates of mutant protein appear progressively in dendrites, in periaxonal processes of oligodendrocytes, and in neuronal and astrocytic perikarya of mice expressing the SOD1(G93A) mutation of familial amyotrophic lateral sclerosis. *J. Neurol. Sci. 177*, 114–123.
18. Stieber, A., Gonatas, J. O., and Gonatas, N. K. (2000) Aggregation of ubiquitin and a mutant ALS-linked SOD1 protein correlate with disease progression and fragmentation of the Golgi apparatus. *J. Neurol. Sci. 173*, 53–62.
19. Jonsson, P. A., Graffmo, K. S., Andersen, P. M., Brannstrom, T., Lindberg, M., Oliveberg, M., and Marklund, S. L. (2006) Disulphide-reduced superoxide dismutase-1 in CNS of transgenic amyotrophic lateral sclerosis models. *Brain 129*, 451–464.
20. Lindberg, M. J., Bystrom, R., Boknas, N., Andersen, P. M., and Oliveberg, M. (2005) Systematically perturbed folding patterns of amyotrophic lateral sclerosis (ALS)-associated SOD1 mutants. *Proc. Natl. Acad. Sci. U.S.A. 102*, 9754–9759.
21. Hart, P. J., Liu, H. B., Pellegrini, M., Nersissian, A. M., Gralla, E. B., Valentine, J. S., and Eisenberg, D. (1998) Subunit asymmetry in the three-dimensional structure of a human CuZnSOD mutant found in familial amyotrophic lateral sclerosis. *Protein Sci. 7*, 545–555.
22. Banci, L., Bertini, I., Cramaro, F., Del Conte, R., Rosato, A., and Viezzoli, M. S. (2000) Backbone dynamics of human Cu,Zn superoxide dismutase and of its monomeric F50E/G51E/E133Q mutant: The influence of dimerization on mobility and function. *Biochemistry 39*, 9108–9118.
23. Hayward, L. J., Rodriguez, J. A., Kim, J. W., Tiwari, A., Goto, J. J., Cabelli, D. E., Valentine, J. S., and Brown, R. H. (2002) Decreased metallation and activity in subsets of mutant superoxide dismutases associated with familial amyotrophic lateral sclerosis. *J. Biol. Chem. 277*, 15923–15931.
24. Rodriguez, J. A., Valentine, J. S., Eggers, D. K., Roe, J. A., Tiwari, A., Brown, R. H., Jr., and Hayward, L. J. (2002) Familial amyotrophic lateral sclerosis-associated mutations decrease the thermal stability of distinctly metallated species of human copper/zinc superoxide dismutase. *J. Biol. Chem. 277*, 15932–15937.
25. Lindberg, M. J., Tibell, L., and Oliveberg, M. (2002) Common denominator of Cu/Zn superoxide dismutase mutants associated with amyotrophic lateral sclerosis: Decreased stability of the apo state. *Proc. Natl. Acad. Sci. U.S.A. 99*, 16607–16612.
26. Fridovich, I. (1995) Superoxide Radical and Superoxide Dismutases. *Annu. Rev. Biochem. 64*, 97–112.
27. Pardo, C. A., Xu, Z. S., Borchelt, D. R., Price, D. L., Sisodia, S. S., and Cleveland, D. W. (1995) Superoxide-Dismutase Is an Abundant Component in Cell-Bodies, Dendrites, and Axons of Motor-Neurons and in a Subset of Other Neurons. *Proc. Natl. Acad. Sci. U.S.A. 92*, 954–958.
28. Tainer, J. A., Getzoff, E. D., Richardson, J. S., and Richardson, D. C. (1983) Structure and Mechanism of Copper, Zinc Superoxide-Dismutase. *Nature 306*, 284–287.
29. Parge, H. E., Hallewell, R. A., and Tainer, J. A. (1992) Atomic Structures of Wild-Type and Thermostable Mutant Recombinant Human Cu,Zn Superoxide-Dismutase. *Proc. Natl. Acad. Sci. U.S.A. 89*, 6109–6113.
30. Hallewell, R. A., Imlay, K. C., Lee, P., Fong, N. M., Gallegos, C., Getzoff, E. D., Tainer, J. A., Cabelli, D. E., Tekampolson, P., Mullenbach, G. T., and Cousens, L. S. (1991) Thermostabilization of Recombinant Human and Bovine CuZn Superoxide Dismutases by Replacement of Free Cysteines. *Biochem. Biophys. Res. Commun. 181*, 474–480.
31. Hallewell, R. A., Masiarz, F. R., Najarian, R. C., Puma, J. P., Quiroga, M. R., Randolph, A., Sanchezpescador, R., Scandella, C. J., Smith, B., Steimer, K. S., and Mullenbach, G. T. (1985) Human Cu/Zn Superoxide-Dismutase cDNA: Isolation of Clones Synthesizing High-Levels of Active or Inactive Enzyme from an Expression Library. *Nucleic Acids Res. 13*, 2017–2034.
32. Hallewell, R. A., Mills, R., Tekampolson, P., Blacher, R., Rosenberg, S., Otting, F., Masiarz, F. R., and Scandella, C. J. (1987) Amino Terminal Acetylation of Authentic Human Cu,Zn Superoxide-Dismutase Produced in Yeast. *Nat. Biotechnol. 5*, 363–366.
33. Fujii, J., Myint, T., Seo, H. G., Kayanoki, Y., Ikeda, Y., and Taniguchi, N. (1995) Characterization of Wild-Type and Amyotrophic Lateral Sclerosis-Related Mutant Cu,Zn-Superoxide Dismutases Overproduced in Baculovirus-Infected Insect Cells. *J. Neurochem. 64*, 1456–1461.
34. Valentine, J. S., and Gralla, E. B. (1997) Biochemistry: Delivering copper inside yeast and human cells. *Science 278*, 817–818.
35. Bartnikas, T. B., and Gitlin, J. D. (2001) How to make a metalloprotein. *Nat. Struct. Biol. 8*, 733–734.
36. Ahl, I. M., Lindberg, M. J., and Tibell, L. A. E. (2004) Coexpression of yeast copper chaperone (yCCS) and CuZn-superoxide dismutases in *Escherichia coli* yields protein with high copper contents. *Protein Expression Purif. 37*, 311–319.
37. Rodriguez, J. A., Shaw, B. F., Durazo, A., Sohn, S. H., Doucette, P. A., Nersissian, A. M., Faull, K. F., Eggers, D. K., Tiwari, A., Hayward, L. J., and Valentine, J. S. (2005) Destabilization of apoprotein is insufficient to explain Cu,Zn-superoxide dismutase-linked ALS pathogenesis. *Proc. Natl. Acad. Sci. U.S.A. 102*, 10516–10521.
38. Shaw, B. F., Durazo, A., Nersissian, A. M., Whitelegge, J. P., Faull, K. F., and Valentine, J. S. (2006) Local unfolding in a destabilized, pathogenic variant of superoxide dismutase 1 observed with H/D exchange and mass spectrometry. *J. Biol. Chem. 281*, 18167–18176.
39. Shaw, B. F., and Valentine, J. S. (2007) How do ALS-associated mutations in superoxide dismutase 1 promote aggregation of the protein? *Trends Biochem. Sci. 32*, 78–85.
40. Chattopadhyay, M., Durazo, A., Sohn, S. H., Strong, C. D., Gralla, E. B., Whitelegge, J. P., and Valentine, J. S. (2008) Initiation and elongation in fibrillation of ALS-linked superoxide dismutase. *Proc. Natl. Acad. Sci. U.S.A. 105*, 18663–18668.
41. Shipp, E. L., Cantini, F., Bertini, I., Valentine, J. S., and Banci, L. (2003) Dynamic properties of the G93A mutant of copper-zinc superoxide dismutase as detected by NMR spectroscopy: Implications for the pathology of familial amyotrophic lateral sclerosis. *Biochemistry 42*, 1890–1899.
42. Banci, L., Bertini, I., Cramaro, F., Del Conte, R., and Viezzoli, M. S. (2002) The solution structure of reduced dimeric copper zinc superoxide dismutase: The structural effects of dimerization. *Eur. J. Biochem. 269*, 1905–1915.
43. Englander, S. W., Mayne, L., Bai, Y., and Sosnick, T. R. (1997) Hydrogen exchange: The modern legacy of Linderstrom-Lang. *Protein Sci. 6*, 1101–1109.
44. Bai, Y. W., Milne, J. S., Mayne, L., and Englander, S. W. (1993) Primary Structure Effects on Peptide Group Hydrogen-Exchange. *Proteins: Struct., Funct., Genet. 17*, 75–86.
45. Jaswal, S. S., and Miranker, A. D. (2007) Scope and utility of hydrogen exchange as a tool for mapping landscapes. *Protein Sci. 16*, 2378–2390.
46. Strange, R. W., Antonyuk, S. V., Hough, M. A., Doucette, P. A., Valentine, J. S., and Hasnain, S. S. (2006) Variable metallation of human superoxide dismutase: Atomic resolution crystal structures of Cu-Zn, Zn-Zn and as-isolated wild-type enzymes. *J. Mol. Biol. 356*, 1152–1162.
47. Valentine, J. S., Doucette, P. A., and Potter, S. Z. (2005) Copper-zinc superoxide dismutase and amyotrophic lateral sclerosis. *Annu. Rev. Biochem. 74*, 563–593.
48. Rakhit, R., Crow, J. P., Lepock, J. R., Kondejewski, L. H., Cashman, N. R., and Chakrabartty, A. (2004) Monomeric Cu,Zn-superoxide dismutase is a common misfolding intermediate in the oxidation models of sporadic and familial amyotrophic lateral sclerosis. *J. Biol. Chem. 279*, 15499–15504.
49. Ermilova, I. P., Ermilova, V. B., Levy, M., Ho, E., Pereira, C., and Beckman, J. S. (2005) Protection by dietary zinc in ALS mutant G93A SOD transgenic mice. *Neurosci. Lett. 379*, 42–46.